Received: 29 June 2016 | Revised: 20 January 2017 | Accepted: 7 June 2017

DOI: 10.1002/asmb.2266

SPECIAL ISSUE PAPER

WILEY

A nondisruptive reliability approach to assess the health of microseismic sensing networks

D. Neira[1] | G. Soto[1] | J. Fontbona[1] | J. Prado[1] | S. Gaete[2]

[1]Center for Mathematical Modeling, Universidad de Chile, Santiago, Chile

[2]Codelco Chile, División El Teniente

Correspondence
Daniel Neira, Center for Mathematical Modeling, Universidad de Chile, Santiago, Chile.
Email: dneira@dim.uchile.cl

Funding information
Codelco Chile, División El Teniente; Basal-Conicyt Grant "Center for Mathematical Modeling" (CMM), Universidad de Chile

Microseismic sensing networks are important tools for the assessment and control of geomechanical hazards in underground mining operations. In such a setting, the maintenance of a healthy network, that is, one that accurately registers all microseisms above some minimum energy level with acceptable levels of noise, is crucially relevant.

In this paper, we develop a nondisruptive method to monitor the health of such a network, by associating with each sensor a set of performance indexes, inspired from reliability engineering, which are estimated from the set of registered signals. Our method addresses 2 relevant features of each of the sensors' behavior, namely, what type of noise is or might be affecting the registering process, and how effective at registering microseisms the sensor is.

The method is evaluated through a case study with microseismic data registered at the Chilean underground mine El Teniente. This study illustrates our method's capability to discriminate and rank sensors with satisfactory, poor, or defective sensing performances, as well as to characterize their failure profile or type, an information that can be used to plan or optimize the network maintenance procedures.

KEYWORDS

reliability engineering, seismic network health, system health monitoring, underground mining

1 | INTRODUCTION

Evaluating and managing the risk due to potential hazards is fundamental for the development of every industrial activity. Being able to identify increasing dangers allows for a timely risk management, securing the safety of workers and minimizing the production delay, as well as all the associated costs.

In the case of underground mining, monitoring anomalous microseismic activity provides a powerful tool to assess hazards related to potential geomechanical instabilities, see Ge.[1] Mendecki et al[2] discuss several specific objectives of seismic monitoring in mines, among which are location of potential rock bursts, prevention of situations unforeseen in the design process, control and regulation of local working activities based on the rock stability, warnings based on the detection of changes in seismic parameters, and back-analysis of anomalous seismic activity in delimited regions of the mine. Therefore, disposing of networks of seismic sensors, which provide information that is both reliable and of high quality, is crucial for secure operation in large-scale underground mines.

If we understand the "health" of a seismic sensor network as its capability to properly register all the microseisms above a certain minimum energy level, and to do this with acceptable levels of noise, it is then clear that a healthy seismic network is a critical tool for risk assessment and management in underground mining operations. In this paper, we introduce a novel nondisruptive method to assess the health of a seismic network of remote sensors. Our approach is based on considering the

networks as a general system and addresses its health as in the framework of system health monitoring.[3] Much of the ideas that we propose could thus also be applied in other industrial settings, where monitoring relies on systems of networks of remote sensors as well and where disruptive monitoring turns out to be too expensive or unfeasible.

The literature on network health assessment is diverse and relies on different points of view, depending on the context. Many of the existing approaches require different levels of disruption in the measuring process (from the step of the sensors and monitoring network design to the step of data processing) and require different levels of understanding of what is being measured. For example, in Ge,[1] the author evaluates the quality of a microseismic network focusing in its accuracy and reliability locating the source of seismic events. The author emphasizes the planning of the monitoring system and its data processing (noise filtering and identification of the arrival of P- and S-waves). In Meng et al,[4] the authors propose a method for network's data collection on the basis of contour maps that can be used as a diagnosis tool to examine the network's health (energy status) and to detect faulty sensors (the ones that report data that is inconsistent with their neighbors').

Dealing directly with uncertainty, linking it with how reliable a sensor's measure is, is another way to address the network's and sensors' health. For example, in Mengshoel et al,[5] the authors adopt a probabilistic approach to diagnose the sensor's health and failures by means of Bayesian networks.[6] Their goal is to validate the sensors and their measurements, to decide whether they have failed or not. Another example is presented in Elouedi et al,[7] where the authors use weighted belief functions in the context of the transferable belief model[8] to account for how reliable a sensor's measurements are. Their supporting idea is to compare the readings of the sensors with the user's knowledge about the real values by minimizing an error function to obtain such weights. Both of these approaches are focused on discrete or categorical measurements.

Lastly, another approach is to view the topic from the electronic perspective. In Xie and Pecht,[9] the authors introduce a methodology to monitor the health of integrated circuits based on measurements of in situ environmental and loading conditions. That procedure requires a good understanding on how those conditions could make sensors fail.

Broadening the list of methodologies to assess the health of a network, the method that we propose is based on ideas that come from reliability engineering. Two of the key characteristics of our method are that it is conceptually simple and that it performs its task in a nondisruptive way, namely, by using only the sensors' readings. This means that our method can be applied to diagnose the health of existing networks using data that is already available as part of their ongoing registering process. Our method is tested on real data obtained from the seismic network of Codelco El Teniente, one of the world's largest underground copper mines.[10,11]

The remainder of the paper is organized as follows. We describe the problem in Section 2, defining relevant concepts and giving some theoretical background in Section 3. In Section 4, we explain the method we developed, showing in Section 5 the results of a goodness-of-fit test and how the mean squared error of our method compares to the Cramér-Rao lower bound. Then, in Section 6, we show the results obtained when applying our method to data from Codelco El Teniente mine, analyzing them in Section 7. Finally, in Sections 8 and 9, we discuss the future research in this topic and conclude, respectively.

2 | DESCRIPTION OF THE PROBLEM

In this paper, we propose a formal conceptual framework to the problem of monitoring the health of a seismic network, motivated by 2 main questions raised by the practical operation and needs of the network:

1. How to evaluate and monitor the performance of each seismic sensor?
2. How to identify the seismic sensors that systematically do not provide useful information?

The network of remote sensors can err in their registering process in 2 ways, which can be seen as an analogy to Types I and II errors of statistical hypothesis testing:

1. Type I error: One or several sensors record a seismogram, yet there is not a real microseism to be registered.
2. Type II error: A microseism occurs, but the network or an individual sensor do not register it.

With this idea in mind, we can reformulate the problem into the next 2 more specific questions:

- Are some seismic sensors repeatedly misidentifying noise as seismic signals?
- Are all sensors recording the seismic activity they are supposed to register?

To address the first question, we will model the performance of a given sensor, based on the relevance of noise in their registering process, ie, how often is noise affecting its ability to register useful data. We do this within the framework of reliability engineering,[12] modeling the noise in their readings as "failures," which we study and treat in a statistical manner. With this

information, we can rank the sensors, identifying the ones that are performing as planned and the ones that systematically do not provide useful or reliable information.

As regards the second question, that is, the ability of a sensor to register the microseisms it is supposed to record, we follow this premise: If a group of sensors record a microseism, all the sensors in some vicinity should have had registered it too. Thus, by identifying those sensors that do not register signals, during one or several of the many microseisms produced every day, we can infer what sensors do systematically not accomplish their task.

3 | BACKGROUND

3.1 | Definitions

We introduce some definitions related to seismic monitoring, which will be used throughout the paper:

- *Sensor* or *site*: an individual device that is used to register seismic movements. It could be a geophone or accelerometer, and it could be uniaxial or triaxial.
- *Seismogram*: corresponds to a signal that represents the movement of the ground in one of the Cartesian directions (x, y, or z) as a function of time.
- *Activation*: When a sensor detects what is supposed to be a microseism and records a signal, we say it has been activated. The exact time at which an activation occurs will be of great importance for the method we shall develop, since our procedure will use, as information, the time lengths between specific activations.
- *Satisfactory activation*: is an activation of a sensor with at least one recorded seismogram that has acceptable levels of noise.
- *Noisy activation*: corresponds to a seismogram with such high level of noise that we cannot tell if there is a real seismic signal or not. In terms of reliability engineering, the noisy activations correspond to the "failures" of the system.
- Δt_{noise}: Given a sensor, the data that we will process correspond to the time differences of its consecutive noisy activations, sorted in ascending order. We call the set of these time differences $\Delta t_{\text{noise}} = \{t_1, t_2, \dots\}$, where the t_i are the increasingly arranged interactivation time lengths.

3.2 | Some reliability engineering ideas and concepts

To approach the monitoring of the health of a microseismic network, we propose to describe and characterize the faulty behavior of each sensor, in analogy with standard ideas and methods of reliability theory. If we understand a noisy activation as a failure of the seismic sensing system and we model the sensors of the network as not being redundant themselves, assuming moreover that times elapsed between each sensor's failures are independent, our problem falls into the setting of reliability models, see Birolini.[12]

In that context, as discussed in Weibull,[13] the Weibull models can be applied to a large group of problems where an event occurring in one part of a system affects the system as a whole. In this spirit, Prabhakar Murthy et al[14] state that these models are suitable for modeling failure data sets and in particular, the "failure times" of different large systems.

In addition, the Weibull distribution is a flexible model for random failure occurrence times and can be easily interpreted in terms of standard key performance indicators. This suggests that it can be useful to tackle the problem that we address here and more precisely, to fit the data in the sets Δt_{noise}.

We next recall some basic objects and concepts in reliability engineering,[12] which will be useful for the method that we will propose.

- Two-parameter Weibull distribution: Denoted as $\mathcal{W}(\boldsymbol{\theta})$, its probability distribution with density function $f(t;\boldsymbol{\theta})$ is defined as follows:

$$f(t;\boldsymbol{\theta}) = \frac{\beta}{\eta}\left(\frac{t}{\eta}\right)^{\beta-1} e^{-\left(\frac{t}{\eta}\right)^{\beta}}, \tag{1}$$

  where $\boldsymbol{\theta} = (\beta, \eta)^{\top}$, $\beta > 0$ corresponds to the shape parameter (dimensionless) and $\eta > 0$ to the scale parameter (time units).
- Cumulative probability: Denoted as $F(t)$, it is defined as the cumulative probability of having a failure within the interval $]0, t[$. In the case of the Weibull distribution, it is given by

$$F(t) = 1 - e^{-\left(\frac{t}{\eta}\right)^{\beta}}. \tag{2}$$

- Reliability: The reliability of an item at time t, denoted $R(t)$, is defined as the probability of not of having a failure within the interval $]0, t[$.

$$R(t) = 1 - F(t) = e^{-\left(\frac{t}{\eta}\right)^{\beta}}. \tag{3}$$

4 | METHODS

4.1 | Fitting a Weibull distribution to the set Δt_{noise}

To evaluate the incidence of noise in the sensors' recordings, we first need to identify the potential sources of noisy activations. As in Ge,[1] when registering microseisms in the underground mining context, we identify 3 main sources of noise:

1. Electric noise: noise at the power line frequency of the alternating current, and its harmonics.
2. Cultural noise: This is the noise produced by the activity within the mine. We assume that it is a high-frequency noise.
3. Measurement noise: This noise is related to the measuring process itself. We assume that this is background noise whose frequencies cannot be determined beforehand.

Once the noisy activations and the types of noise have been identified, we can fit a Weibull distribution to the corresponding points in Δt_{noise}, via maximum likelihood estimation.

With the parameters of the distribution being estimated, we can then compute the reliability of each sensor with respect to the different types of noise using (3).

4.1.1 | Estimation of noise

To estimate the noise that is present in the seismograms, we propose 3 indicators, one for each type of noise.

In each case, we can compare the computed value of the indicator with a threshold to determine whether an activation is noisy or not.

To ease the presentation, we begin by giving the definition of the power spectral density (PSD). We then proceed with the definitions of the three indicators, two of which will heavily depend on the PSD.

Let a real-valued seismic signal $x[n]$ be a wide-sense stationary random process that is bandlimited in the frequency domain, ie, its support is bounded in that space.

We are interested in the problem of estimating the power of $x[n]$, for which the PSD can be used. The PSD allows us to characterize the power of signals like $x[n]$, describing how its power is distributed along the frequency domain.

To estimate the PSD of $x[n]$, we can follow at least 2 paths. On the one hand, we can do it by computing the Fourier transform of the autocorrelation function of $x[n]$, which needs to be estimated too, or, on the other hand, we can do it directly using the periodogram, which can be derived through the autocorrelation function and is introduced next.

Be $\gamma(l)$ the autocorrelation function of $x[n]$, $0 \leqslant n \leqslant N-1$. It can be estimated as follows:

$$\hat{\gamma}(l) = \frac{1}{N}\sum_{j=0}^{N-1} x[j+l]x[l]. \tag{4}$$

As stated before, the PSD can be estimated through the discrete Fourier transform of the autocorrelation function. That is,

$$\widehat{\text{PSD}}(f_k) = \mathcal{F}\{\hat{\gamma}(l)\} = \sum_{l=-N}^{N} \hat{\gamma}(l) e^{-2\pi \frac{f_k}{f_s} l}, \tag{5}$$

where f_s is the sampling frequency.

Using (4) and (5), we get

$$\widehat{\text{PSD}}(f_k) = \frac{1}{N}\sum_{l=-N}^{N}\left(\sum_{j=0}^{N-1} x[j+l]x[l]\right) e^{-2\pi \frac{f_k}{f_s} l}, \tag{6}$$

expression that after some algebraic manipulations leads to

$$\widehat{\mathrm{PSD}}(f_k) = \frac{1}{N}|X[f_k]|^2, \tag{7}$$

where $|X[f_k]|^2$ is the discrete Fourier transform of $x[n]$.

This estimator of the PSD is known as the periodogram, so we can rewrite (7) as

$$\widehat{\mathrm{PSD}}(f_k) = \mathrm{Periodogram}(x[n]) = \frac{1}{N}|X[f_k]|^2. \tag{8}$$

We wish to estimate the PSD by means of the periodogram. Now, given that this estimator is susceptible to large uncertainties,[15] it is necessary to reduce its variance. We accomplish this multiplying the seismic signal with a suitable window to minimize the maximum sidelobes of the periodogram:

$$\widehat{\mathrm{PSD}}(f_k) = \mathrm{Periodogram}(x[n]w[n]) = \frac{1}{N}|X[f_k] * W[f_k]|^2, \tag{9}$$

where $*$ denotes convolution and $W[f_k]$ is the discrete Fourier transform of $w[m]$, the Nuttall's 4-term Blackman-Harris window,[16] given in the discrete-time domain by

$$\begin{aligned} w[m] = a_0 - a_1 \cos\left(2\pi\frac{m}{M-1}\right) + \\ a_2 \cos\left(4\pi\frac{m}{M-1}\right) - a_3 \cos\left(6\pi\frac{m}{M-1}\right), \end{aligned} \tag{10}$$

with m the window sample, $0 \leqslant m \leqslant M-1$, where M is the window length, and $a_0 = 0.3635819$, $a_1 = 0.4891775$, $a_2 = 0.1365995$, and[16] $a_3 = 0.0106411$. The peak-sidelobes of this window are at level -98.17 dB, so the filter reduces the variance of the periodogram effectively.

Now, we proceed to present the 3 proposed indicators.

Electric noise meter

The electric noise meter (ENM) measures the electric noise energy contribution of a discrete-time signal with respect to the total energy and is estimated as follows:

$$\widehat{\mathrm{ENM}} = 100\frac{\sum\limits_{f\in\Lambda}\widehat{\mathrm{PSD}}(f)}{\sum\limits_{0<f\leqslant f_{\mathrm{lim}}}\widehat{\mathrm{PSD}}(f)}, \tag{11}$$

where $\Lambda = \{mf_0 : m = 1, 2, \ldots, M\}$ is the set of the power line frequency $f_0 = 50$ Hz ($f_0 = 60$ Hz in some countries) and M of its harmonics, $\widehat{\mathrm{PSD}}$ stands for the estimated power spectral density of the signal, and f_{lim} represents the highest frequency to be analyzed and is such that

$$Mf_0 \leqslant f_{\mathrm{lim}}. \tag{12}$$

The value of f_{lim} is determined by the conditions of the problem at hand and the Nyquist-Shannon sampling theorem, which establishes a sufficient condition that guarantees that a discrete-time sequence obtained from a continuous signal is able to capture all the information available in it.

The sampling theorem can be described as follows. Let F_m denote the largest frequency of interest in the continuous signal, and F_s be the sampling frequency (the rate at which the signal is sampled). Then, the theorem states that the continuous-time signal can be reconstructed from its samples provided that[17]

$$F_s \geqslant 2F_m. \tag{13}$$

In our case, the lowest sampling rate associated with El Teniente's seismic network corresponds to $F_s = 2$ kHz, so we set the maximum frequency to be analyzed as $F_m = f_{\mathrm{lim}} = 1$ kHz due to (13), fixing then $M = 20$ due to (12).

Also, the fact that in (11) are being considered only the frequencies that are greater than zero is because we are analyzing a real-valued signal, and the spectral content of such signals is conjugate symmetric in the Fourier domain.

The PSD is estimated as described before.

High-frequency noise ratio

We use the high-frequency noise ratio (HFNR) to quantify the cultural noise level. It represents the difference (in decibels) between the power of the seismic signal P_X and the power of the high frequency noise P_R, ratio that is estimated as follows:

$$\widehat{\text{HFNR}} = 10 \log_{10} \left(\frac{\hat{P}_X}{\hat{P}_R} \right). \tag{14}$$

To estimate the power of a discrete-time signal $y[n]$ over the interval $0 \leqslant n \leqslant N-1$, we can use

$$\widehat{\text{Power}}_y = \frac{1}{N} \sum_{n=0}^{N-1} |y[n]|^2. \tag{15}$$

However, there are some cases where it is more convenient to perform this estimation in the frequency domain by means of Parseval's theorem,[18] which allows us to write (15) as follows:

$$\widehat{\text{Power}}_y = \frac{1}{N^2} \sum_{k=0}^{N-1} |Y[f_k]|^2 = \frac{1}{N} \sum_{k=0}^{N-1} \widehat{\text{PSD}}_y(f_k), \tag{16}$$

where $Y[f_k]$ is the discrete Fourier transform of $y[n]$ and where we have identified that $|Y[f_k]|^2/N$ is the same as the periodogram of the power spectral density of $y[n]$ at f_k.

Using (16) and the fact that both P_X and P_R have the same number of samples N, we can calculate (14) in terms of the PSD:

$$\widehat{\text{HFNR}} = 10 \log_{10} \left(\frac{\sum_k \widehat{\text{PSD}}_X(f_k)}{\sum_k \widehat{\text{PSD}}_R(f_k)} \right). \tag{17}$$

Up to this point, we still need to identify which part of the data corresponds to the seismic signal and which to high frequency noise.

To do this, we rely on the fact that, as seismic signals are transient signals, they only occur in a small part of the total data.[19] With this in mind, we extract the seismic signal from the data using a low-pass filter with cutoff frequency f_c. That is, we associate the seismic signal with the spectral content that is in the set $\Phi = \{f : 0 < f \leqslant f_c\}$, and the high frequency noise to the frequencies that do not belong to Φ.

This consideration allows us to rewrite (17) in the form we finally use to estimate the indicator:

$$\widehat{\text{HFNR}} = 10 \log_{10} \left(\frac{\sum_{f \in \Phi} \widehat{\text{PSD}}(f)}{\sum_{f \notin \Phi} \widehat{\text{PSD}}(f)} \right). \tag{18}$$

The cutoff frequency f_c is chosen as the frequency that accounts for p times the total power:

$$\sum_{f_k > 0}^{f_c(p)} \widehat{\text{PSD}}(f_k) = p \cdot \sum_{f_k > 0}^{F_s/2} \widehat{\text{PSD}}(f_k), \tag{19}$$

where $F_s/2$ is the Nyquist frequency as in (13), $f_c(p)$ represents the value that we are looking for as a function of p, and $0 < p \leqslant 1$ is the portion of the total accumulated PSD considered. In our case, $p = 0.95$.

We estimate the PSD in the same way as previously described.

Signal-to-noise ratio

This ratio gives us information about the background noise, ie, the low energy values that are present on the data reading.

Modeling the background noise as

$$\begin{matrix}\text{background} \\ \text{noise}\end{matrix} = \begin{matrix}\text{electric} \\ \text{noise}\end{matrix} + \begin{matrix}\text{cultural} \\ \text{noise}\end{matrix} + \begin{matrix}\text{measurement} \\ \text{noise}\end{matrix}, \tag{20}$$

we estimate the measurement noise computing the SNR of a seismogram whose electric and cultural noises have been filtered out.

The signal-to-noise ratio (SNR) is defined as

$$\text{SNR} = 10 \log_{10} \left(\frac{P_X}{P_N} \right), \tag{21}$$

and represents the difference (in decibels) between the power of the seismic signal P_X and the power of the background noise P_N.

Note that the definitions for the ENM and HFNR can be interpreted as "partials" signal-to-noise measurements to filter the noise in 3 stages, of which the SNR indicator is the last one.

Given that the seismic signals are passband, we can estimate (21) in terms of $\hat{\sigma}_X$ and $\hat{\sigma}_N$, the estimated standard deviations of the signal and the noise, respectively:

$$\widehat{\mathrm{SNR}} = 20 \log_{10}\left(\frac{\hat{\sigma}_X}{\hat{\sigma}_N}\right), \tag{22}$$

where $\hat{\sigma}_X$ is obtained by

$$\hat{\sigma}_X = \sqrt{\frac{1}{T-1}\sum_{t=1}^{T}\left(x_t - \bar{x}\right)^2}, \tag{23}$$

with x_t the noisy signal, $\bar{x}$ the mean, and T the sample size.

As the value of σ_N is unknown, we propose a Monte Carlo[20] method to calculate the $\widehat{\mathrm{SNR}}$:

1. We take R samples of size L from the seismogram data, with replacement, in random time instants. In this way, we obtain $\tau_r = \{t_l\}_{l=0}^{L-1}$, the set of time instants of the r-th sample, where $t_l \in [0, n-1]$, $r \in [0, R-1]$, and n represents the length of the signal.

   In our case, following Ata,[21] we calculate L with

$$L = \left(\frac{z_{\alpha/2}\cdot\sqrt{p(1-p)}}{e_M}\right)^2 \tag{24}$$

   by fixing $(1-\alpha)100 = 95\%$, which corresponds to the confidence level, $\alpha = 5\%$ to the level of significance, $p = 90\%$ to the portion of low energy values we want to consider, and $e_M = 5\%$ to the sampling error.
2. We estimate σ_r, the value of the standard deviation of the r-th sample, with the robust estimator

$$\hat{\sigma}_r = K \cdot \mathrm{MAD}_r, \tag{25}$$

   where K is a scale factor that depends on the underlying distribution, being K =1.4826 for the Gaussian case.

   In the expression (25), MAD_r stands for the median absolute deviation of the r-th sample and is defined as

$$\mathrm{MAD}_r = \mathrm{median}\left(\left|x_{\tau_r} - \mathrm{median}(x_{\tau_r})\right|\right), \tag{26}$$

   which is an effective way to discard outliers in the estimation of the standard deviation of the samples.
3. Finally, we estimate σ_N as the mean of the $\hat{\sigma}_r$,

$$\hat{\sigma}_N = \frac{1}{R}\sum_{r=1}^{R}\hat{\sigma}_r, \tag{27}$$

   then replacing the relevant values in (22) to estimate the SNR.

4.1.2 | Maximum likelihood estimation with leave-one-out cross-validation

Assuming that the noisy interactivation times t_i are i.i.d. random variables, we could estimate $\boldsymbol{\theta} = (\beta, \eta)^\top$ for the 2-parameter Weibull distribution solving

$$\hat{\boldsymbol{\theta}} = \arg\max_{\boldsymbol{\theta}} \ell(\boldsymbol{\theta}; t_1, \ldots, t_n), \tag{28}$$

with

$$\ell(\boldsymbol{\theta}; t_1, \ldots, t_n) = n(\ln\beta - \ln\eta) - \sum_{i=1}^{n}\left(\frac{t_i}{\eta}\right)^{\beta} + (\beta-1)\sum_{i=1}^{n}\ln\left(\frac{t_i}{\eta}\right), \tag{29}$$

the log-likelihood of the $\{t_i\}_{i=1}^n$.

In the case of the 2-parameter Weibull distribution, the maximum likelihood estimation (MLE) experiences a bias problem,[22] but it satisfies the regularity conditions, so it has an unique global maximum $\hat{\boldsymbol{\theta}}$.

To control the bias and reduce the uncertainty in the estimation, we perform leave-one-out (LOO) cross-validation[23] to the $\Delta t_{\mathrm{noise}} = \{t_i : i = 1, 2, \ldots, n\}$, which gives us n estimates for each parameter. To obtain the final estimate $\hat{\boldsymbol{\theta}} = (\hat{\alpha}, \hat{\beta})^\top$, we do the following.

Assuming that the underlying probability density function (*pdf*) associated with the values obtained with LOO for each estimated parameter is smooth, we use kernel density estimation (KDE)[23] with a Gaussian kernel to estimate each of the *pdfs* nonparametrically.

We obtain the final estimate $\hat{\boldsymbol{\theta}}$ computing the mode of each estimated curve as its argument of the maximum by means of the ∞-norm. We approximate this by the p-norm, with $p \gg 1$:

$$\hat{\theta}_k = \arg\max_{\theta\in\Theta} \hat{f}_{\theta_k}(\theta) \approx \frac{\sum_{j=1}^{m} \hat{f}^p_{\theta_k}(\theta_j)\theta_j}{\sum_{j=1}^{m} \hat{f}^p_{\theta_k}(\theta_j)}, \tag{30}$$

where $\hat{f}_{\theta_k}$ represents the underlying *pdf* of θ_k, the parameter whose value we want to estimate, and $\boldsymbol{\Theta}$ is the set of possible values for the parameter. Note that using KDE allows us to calculate the mode with a fine grid of m elements that is independent of n (the number of estimates we have for each parameter), allowing us to choose any suitable $m > n$.

This procedure is summarized in Algorithm 1.

Note that, as we saw in Section 3.2, we can use expression (3) and the estimated parameters of the Weibull distributions to evaluate the reliability of each sensor for each type of noise.

Algorithm 1 Weibull fitting: 2-parameter estimation

Require: The data to be fitted, $\{t_i\}_{i=1}^{N}$, and p as in (30)

procedure WEIBULLFIT(data, p)
  for k in $\{1, \dots, N\}$ **do** ▷ MLE+LOO
    $\{\hat{\beta}_k\}, \{\hat{\eta}_k\} \leftarrow$ Fit a Weibull distribution to $D_k = \{\{t_i\}_{i=1}^{N} \setminus \{t_k\}\}$ by means of MLE.
  end for
  $\{\hat{f}_{\hat{\beta}}\}, \{\hat{f}_{\hat{\eta}}\} \leftarrow$ Estimate, using KDE, the underlying *pdfs* of $\{\hat{\beta}_k\}_{k=1}^{N}$, and $\{\hat{\eta}_k\}_{k=1}^{N}$.
  $\hat{\beta}, \hat{\eta} \leftarrow$ Estimate the parameters of the Weibull distribution computing the mode of each *pdf*.
end procedure

4.2 | Extraction of the ratio of activations

The ratio of activations r_{act} corresponds to the quotient between the number of satisfactory activations registered by a sensor, and the number of satisfactory activations that said sensor was supposed to register, in a given period:

$$r_{\text{act}}\big|_{\text{sID}} = \left.\frac{\begin{array}{c}\#\text{ of satisfactory}\\ \text{activations registered}\end{array}}{\begin{array}{c}\text{total \# of satisfactory activations}\\ \text{that must have been registered}\end{array}}\right|_{\text{sID}}, \tag{31}$$

where # stands for number and "sID" for "site ID", which is unique for each sensor. To estimate r_{act}, we propose the following method.

Given a microseism, we would like to define a volume within which the sensors must have been activated. This will allow us to estimate the total number of satisfactory activations a sensor must have registered as well as to identify the sensors that did not register the microseism. We only proceed doing this when the number of seismograms associated with the satisfactory activations is greater than a user-selected threshold N_r.

Repeating this process for all the microseisms that the network detected, and summing all the instances where a sensor did not register the microseisms that it was supposed to register, we obtain the number of times the sensors failed to register the information.

Adding this value, per sensor, to the number of satisfactory activations, gives us the total of satisfactory activations that the sensors were supposed to register. Finally, we obtain $r_{\text{act}}\big|_{\text{sID}}$ replacing the relevant values in (31).

In practice, for simplicity, we impose the volume to be a sphere whose center is close to the sensors that registered the higher energy seismograms.

To be able to compare the energy associated with sensors that can be uniaxial or triaxial, we would like to have one seismogram per sensor to deal with. To do this, we first filter the seismograms' noise and, for each sensor with satisfactory activations, we calculate a weighted average of their 1-to-3 associated seismograms, obtaining what we call the reduced seismogram per sensor:

$$\bar{q}_m = \frac{\sum_u w_{mu} q_{mu}}{\sum_u w_{mu}}, \tag{32}$$

where q_{mu} is the seismogram of the m-th sensor in the u-axis, $u \in \{\hat{x}, \hat{y}, \hat{z}\}$, and $w_{mu} = \mathbb{V}ar(q_{mu})$, a measure that is proportional to the energy of q_{mu}.

Once we have computed all the relevant $\bar{q}_m$, we calculate $r_{\text{CM}} \in \{x_{\text{CM}}, y_{\text{CM}}, z_{\text{CM}}\}$, the coordinates of the center of the sphere, as if it were the center of mass of a particle system, weighting each of the coordinates of the sensors that registered a satisfactory activation with the "magnitude" of their reduced seismograms:

$$r_{\text{CM}} = \frac{\sum_m \text{mag}(\bar{q}_m) r_{\bar{q}_m}}{\sum_m \text{mag}(\bar{q}_m)}, \tag{33}$$

where $r_{\bar{q}_m}$ is the distance to the origin in the r-th Cartesian coordinate of the m-th sensor that registered a satisfactory activation, and $\text{mag}(\bar{q}_m)$ is the maximum amplitude ("magnitude") of $\bar{q}_m$. Doing this for $r \in \{x, y, z\}$, we obtain $(x_{\text{CM}}, y_{\text{CM}}, z_{\text{CM}})^\top$, the center of the sphere for the given microseism.

Choosing the radius of the sphere is a delicate task. On the one hand, if the sphere is too big, the method might overreact, misidentifying some sensors as no activated. On the other hand, with a small sphere, the method might underestimate the problem, leaving not-activated sensors unidentified.

Acknowledging the compromise between the radius of the sphere and the sensitivity of the method, and when in absence of relevant information to choose it, we propose to determine the radius of the sphere as the distance between its center and the position of the sensor that is halfway to the farthest site that detected the microseism.

4.3 | Incorporation of the reliability and the ratio of activations in a new performance indicator

We next introduce a simple indicator, computed for each individual sensor, and denoted $s|_{\text{sID}}$, that conveys both the information of the reliability of the sensors and their ratio of activations. It is obtained as follows.

First, we compute what we call the reduced reliability for each sensor, per type of noise, with

$$R(t)\Big|_{\substack{\text{sID} \\ \text{noise}}} = \sqrt{\frac{1}{N_{\text{axes}}} \sum_{\text{axis}} \left(R(t)\Big|_{\substack{\text{sID} \\ \text{noise}}}^{\text{axis}} \right)^2}, \tag{34}$$

where N_{axes} stands for the number of axes of the sensor "sID," obtaining 3 reliabilities per sensor: reliability with respect to electric noise, cultural noise, and measurement noise.

Then, we calculate an aggregated reliability per sensor as the mean of the reliabilities described before:

$$R(t)\Big|_{\text{sID}} = \frac{1}{3} \sum_{\text{noise}} R(t)\Big|_{\substack{\text{sID} \\ \text{noise}}}. \tag{35}$$

Finally, we calculate the proposed performance indicator $s\big|_{\text{sID}}$ multiplying the aggregated reliability with the respective ratio of activations:

$$s\big|_{\text{sID}} = R(t)\big|_{\text{sID}} \cdot r_{\text{act}}\big|_{\text{sID}}. \tag{36}$$

5 | GOODNESS-OF-FIT AND ERROR QUANTIFICATION

5.1 | Kolmogorov-Smirnov hypothesis test

When applying the maximum likelihood estimation with LOO procedure (as presented in Section 4.1.2) to the data that will be explained and analyzed in Section 6, we obtain results as the ones in Figures 1 and 2.

For the example depicted in Figure 1, we fitted a Weibull distribution to an actual Δt_{noise} data set obtained from El Teniente's seismic network: in this case, to the data that is associated with the cultural noise present in the z-axis of sensor 138, obtaining $\hat{\beta} = 0.7937$ and $\hat{\eta} = 0.0369$.

We did the same procedure for Figure 2, now for the set Δt_{noise} that is associated with the measurement noise present in the z-axis of sensor 138, obtaining $\hat{\beta} = 0.8496$ and $\hat{\eta} = 0.0319$.

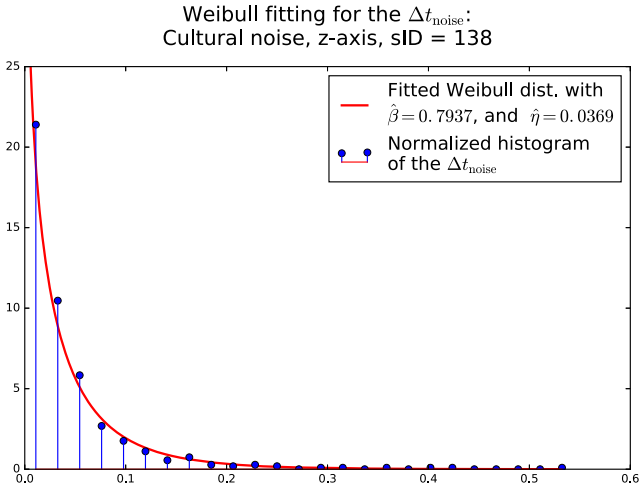

FIGURE 1 Two-parameter Weibull fitting to the corresponding set Δt_{noise} for the cultural noise present in the z-axis of sensor 138. The estimated parameters of the Weibull distribution are $\hat{\beta} = 0.7937$ and $\hat{\eta} = 0.0369$ [Colour figure can be viewed at wileyonlinelibrary.com]

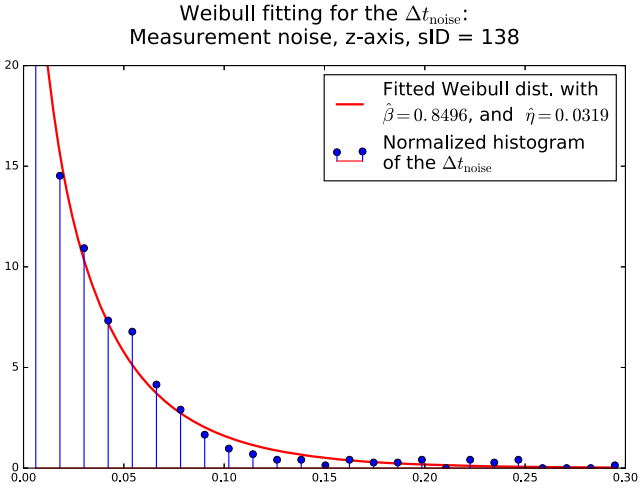

FIGURE 2 Two-parameter Weibull fitting to the corresponding set Δt_{noise} for the measurement noise present in the z-axis of sensor 138. The estimated parameters of the Weibull distribution are $\hat{\beta} = 0.8496$ and $\hat{\eta} = 0.0319$ [Colour figure can be viewed at wileyonlinelibrary.com]

From the figures, we can see that the 2-parameter Weibull distribution fits the purpose of modeling different sets of Δt_{noise}.

To confirm this visual appreciation, we performed the Kolmogorov-Smirnov goodness-of-fit hypothesis test for Weibull distributions with estimated parameters as described in D'Agostino and Stephens.[24]

The hypothesis of the test are as follows:

- H_0: The data do come from the estimated Weibull distribution $\mathcal{W}(\hat{\boldsymbol{\theta}})$.
- H_1: The data is not distributed as $\mathcal{W}(\hat{\boldsymbol{\theta}})$.

The test statistic is $\sqrt{n}D_n$, where n is the sample size and $D_n = \sup_x \left|\hat{F}_n(x) - \hat{F}(x)\right|$, with $\hat{F}$ the *cdf* of the fitted distribution, $\hat{F}_n$ the *cdf* of the empirical distribution, and $\sup_x$ the supremum of the distances.

In the case of the fit depicted in Figure 1, we obtained $\sqrt{n}D_n = 0.7689$, whereas $\sqrt{n}D_n = 0.7905$ was obtained for the case of Figure 2. Since these values are smaller than $\sqrt{n^*}D_{n^*} = 0.803$, the smallest critical value given in D'Agostino and Stephens[24] [Table 4.18] for $n^* > 50$, in both cases, there is not enough evidence to reject the null hypothesis, confirming that the data Δt_{noise} can be explained as being sampled from the estimated Weibull distribution.

5.2 | Cramér-Rao lower bound

To quantify how our method of estimation behaves, we compare its mean squared error (MSE) with the Cramér-Rao lower bound (CRLB) that is associated with the estimation of $\boldsymbol{\theta}$ for the 2-parameter Weibull distribution. The CRLB specifies the

lowest possible variance for an estimator, giving us the benchmark to compare to. We do this comparison for different sample sizes.

The closed-form expression of the CRLB for the 2-parameter Weibull distribution can be obtained calculating the elements of the Fisher Information Matrix:

$$(\mathcal{I}(\boldsymbol{\theta}))_{i,j} = -\mathbb{E}\left[\frac{\partial^2}{\partial\theta_i\partial\theta_j}\ln f(X;\boldsymbol{\theta})\middle|\boldsymbol{\theta}\right], \tag{37}$$

where $\boldsymbol{\theta} = (\beta,\eta)^\top$, and $f(X;\boldsymbol{\theta})$ is the *pdf* of the Weibull distribution $\mathcal{W}(\boldsymbol{\theta})$.

Following Newby,[25] the expected values in (37) are

$$\mathbb{E}\left\{\frac{\partial^2\ell}{\partial\beta^2}\right\} = -\frac{1}{\beta^2}\left[1+\Gamma''(2)\right], \tag{38}$$

$$\mathbb{E}\left\{\frac{\partial^2\ell}{\partial\eta^2}\right\} = -\frac{\beta^2}{\eta^2}, \tag{39}$$

$$\mathbb{E}\left\{\frac{\partial^2\ell}{\partial\beta\partial\eta}\right\} = \mathbb{E}\left\{\frac{\partial^2\ell}{\partial\eta\partial\beta}\right\} = -\frac{1}{\eta}\Gamma'(2), \tag{40}$$

where ℓ is the log-likelihood, $\ell = \ln f(\boldsymbol{\theta};X)$, and $\Gamma(.)$ is the gamma function.

Then, inverting (37) and using the expressions (38), (39), and (40), we obtain the Cramér-Rao lower bound for β, and η:

$$\mathrm{CRLB}(\beta) = \frac{6}{N\pi^2}\beta^2, \tag{41}$$

$$\mathrm{CRLB}(\eta) = \frac{6}{N\pi^2}\left[(\gamma-1)^2+\frac{\pi^2}{6}\right]\left(\frac{\eta}{\beta}\right)^2, \tag{42}$$

where γ is the Euler-Mascheroni constant.

To learn how far are the MSEs of our estimations from the CRLB, we propose the following procedure.

We choose $\boldsymbol{\theta} = \boldsymbol{\theta}^\star$, and sample a set of size $m \in \{m_j\}_{j=1}^M$ from $\mathcal{W}(\boldsymbol{\theta}^\star)$. For each sample size, we run R trials in accordance to Algorithm 2. After the R trials, for each sample size and corresponding estimated parameter, we calculate its MSE:

$$\mathrm{MSE}(\hat{\theta}_k) = \mathbb{V}ar(\hat{\theta}_k) + \left(\mathrm{Bias}(\hat{\theta}_k,\theta_k)\right)^2. \tag{43}$$

A comparison of the results obtained when estimating $\boldsymbol{\theta}^\star = (0.687, 0.120)^\top$ for sample sizes 5, 10, 20, 30, 40, 50, 60, 70, 80, 90, and 100, with $R = 1000$, are presented in Figure 3 for β and Figure 4 for η.

Algorithm 2 Method's MSE estimation for sample size m

Require: $\theta^\star = (\beta^\star,\eta^\star)^\top$, p, m, and R

1: **for** r in $\{1,\dots,R\}$ **do**
2: data $= \{t_i\}_{i=1}^m \leftarrow$ Sample a set of m elements, with replacement, from $\mathcal{W}(\beta^\star,\eta^\star)$, arranging them in ascending order.
3: $\hat{\beta}_r, \hat{\eta}_r \leftarrow$ WeibullFit(data, p) as in Algorithm 1.
4: **end for**
5: $\hat{\beta},\hat{\eta} \leftarrow$ Estimate the final parameters as the mean of the R trials, $\hat{\theta} = \frac{1}{R}\sum_{r=1}^R \hat{\theta}_r$.

From the figures, we can see that at a sample size equal or greater than 50, the difference between the values of the MSE and the CRLB is negligible.

6 | APPLICATION

Our methodology was applied to data registered by El Teniente's seismic network on September 8, 2010.

Analyzing every seismogram available in El Teniente's data, we identified 92, 46, and 139 series of noisy activations according to ENM, HFNR, and SNR, respectively. These give us a total of 277 series of noisy activations to work with. Within these series, the minimum of noisy activations or "points" registered is 1, and the maximum is 708.

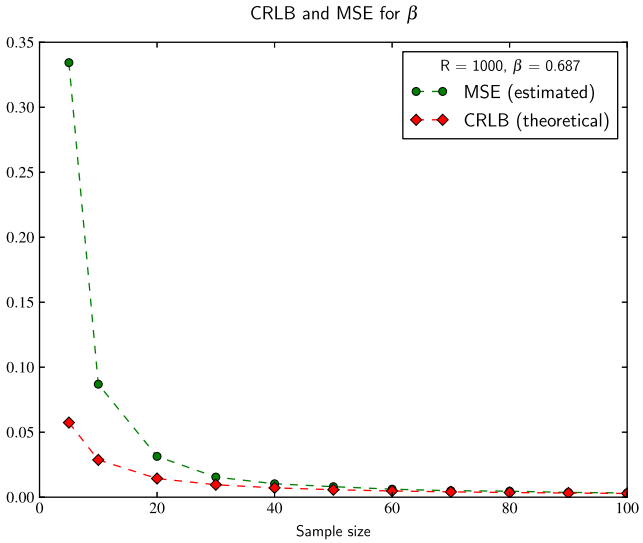

FIGURE 3 Comparison of the mean squared error (MSE) and Cramér-Rao lower bound (CRLB) for the estimation of β, with $\boldsymbol{\theta}^{\star} = (0.687, 0.120)^{\mathsf{T}}$, for different sample sizes, $R = 1000$ trials and $p = 10$ [Colour figure can be viewed at wileyonlinelibrary.com]

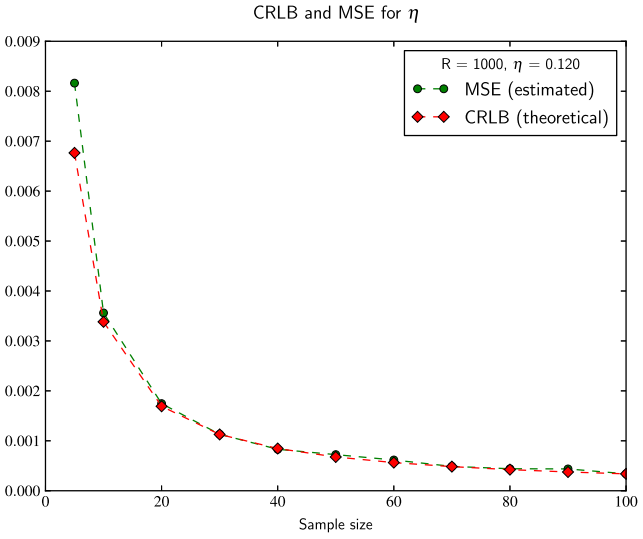

FIGURE 4 Comparison of the MSE and CRLB for the estimation of η, with $\boldsymbol{\theta}^{\star} = (0.687, 0.120)^{\mathsf{T}}$, for different sample sizes, $R = 1000$ trials, and $p = 10$ [Colour figure can be viewed at wileyonlinelibrary.com]

For this application, we chose $u = 50$ (minimum number of points to perform the Weibull fitting), $t^{*} = 0.5$ hours (time, in hours, used to evaluate the reliability indicator), and $N_r = 3$ (minimum number of satisfactory activations to construct the sphere that is necessary to calculate the ratio of activations). The optimization of the log-likelihood was performed through the library `fmin_tnc` of Scipy (Python), which implements a truncated Newton algorithm that uses gradient information.

The choice of $u = 50$ obeys what had been found in Section 5.2: At this sample size, the MSE is close enough to the CRLB, almost reaching the lowest possible variance.

Given all these chosen parameters, 34 and 66 sensors out of 68 had enough data to compute the aggregated reliability and ratio of activations, respectively.

And in the case of the performance indicator s, the number of sensors reduces slightly from 34 to 33. This means that one sensor had enough data to compute $R(t^{*})$, but not r_{act}, the latter because, for each microseism, it did not have at least $N_r = 3$ satisfactory activations.

The obtained results are shown in Figures 5 to 12, and their analysis is presented in Section 7.

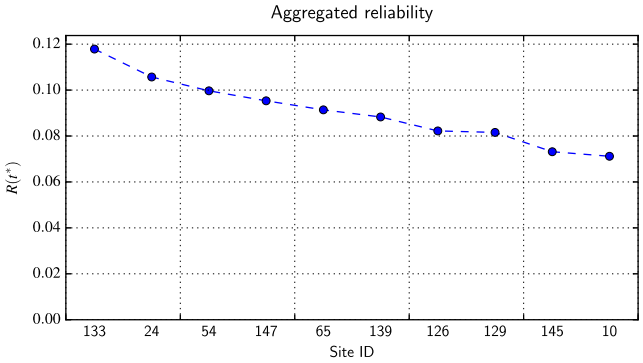

FIGURE 5 Top 10 sensors (from a total of 34) in terms of the aggregated reliability [Colour figure can be viewed at wileyonlinelibrary.com]

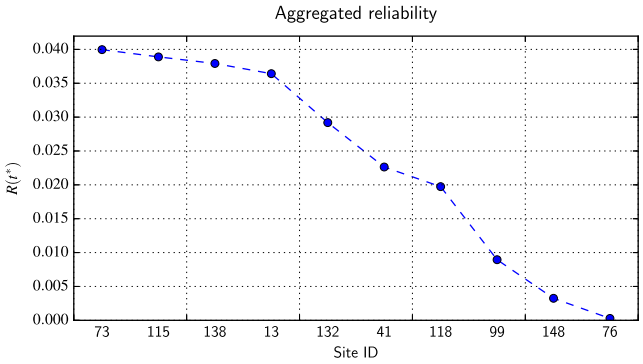

FIGURE 6 The 10 worst sensors in terms of the aggregated reliability. Note the difference in scale in relation to Figure 5 [Colour figure can be viewed at wileyonlinelibrary.com]

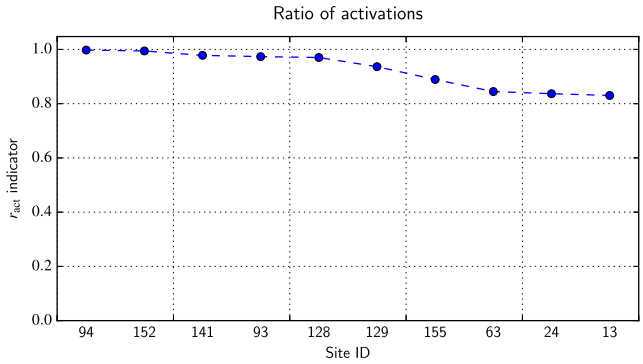

FIGURE 7 Top 10 sensors (from a total of 66) in terms of the ratio of activations [Colour figure can be viewed at wileyonlinelibrary.com]

7 | ANALYSIS

We next analyze the results using 3 indicators: the aggregated reliability $R(t^*)$, the ratio of activations r_{act}, and the s performance indicator, which consolidates the information of $R(t^*)$, and r_{act}.

It is important to keep in mind that the value of each of these indicators depends on the parameters considered when using the method. Notice that they not only rely on u, t^*, N_r but also on the thresholds considered when estimating the different types of noise.

Using different thresholds to decide whether an activation is a noisy one will thus change the results, even when using the same set of data. Changing the approach used to determine the radius of the spheres needed to calculate the ratio of activations will do so too.

All of these parameters are application-specific and need to be chosen beforehand by the experts. It is important to have this in mind when interpreting the results.

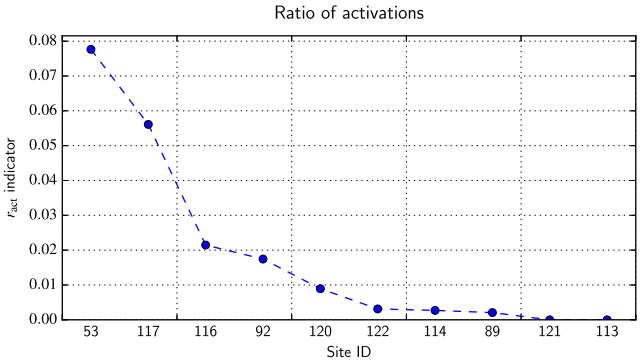

FIGURE 8 The 10 worst sensors in terms of the ratio of activations. Note the big difference between this scale and the one in Figure 7 [Colour figure can be viewed at wileyonlinelibrary.com]

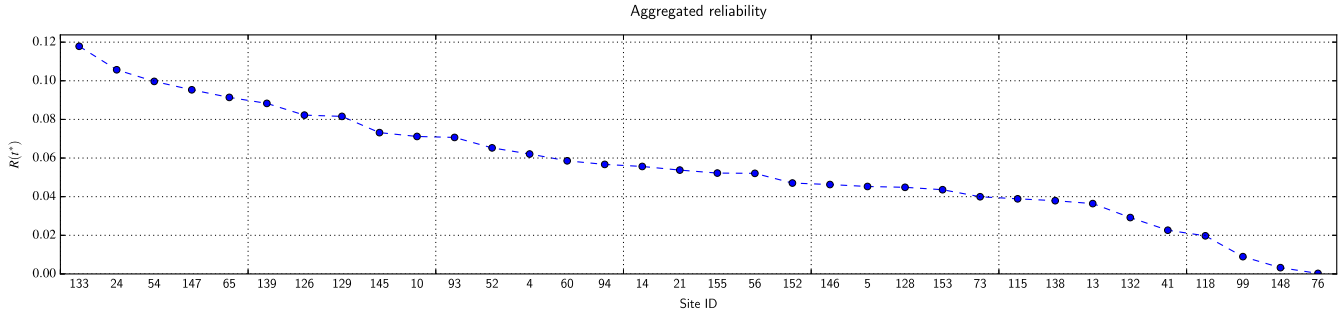

FIGURE 9 Aggregated reliability for all the sensors with suitable data to calculate the indicator [Colour figure can be viewed at wileyonlinelibrary.com]

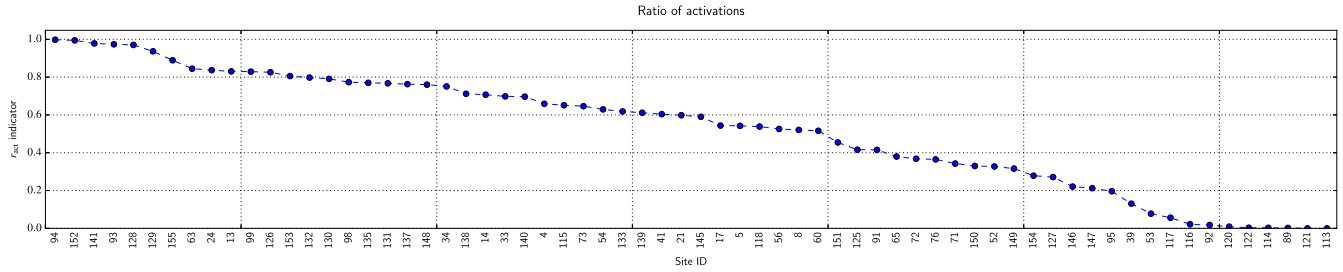

FIGURE 10 Ratio of activations for all the sensors with suitable data to calculate the indicator [Colour figure can be viewed at wileyonlinelibrary.com]

For this particular application, note that we calculate the value of the reliability indicator at $t^* = 0.5$ hours. Then, $R(t^* = 0.5)$ accounts for the probability of not registering a noisy activation during the next 30 minutes. In terms of that probability value, the tolerance to determine what is considered to be a reliable sensor depends on the application in mind.

7.1 | Reliability: $R(t^*)$

Given that $\max\{R(t)\} = 1$, and the fact that the network serves its objective adequately, we can see from Figure 5 that we need to interpret the values of $R(t^*)$ in context.

Consider the said figure: The highest 15% (top 5) sensors reveal an aggregated reliability $R(t^*) \geqslant 0.09$. We might wonder whether this is a satisfactory value for the indicator, question we can only answer in a case by case basis.

In the particular case of our application, we know that the seismic network of Codelco El Teniente accomplishes its task satisfactorily. We choose then to follow a pragmatic approach: We say that the higher ranked sensors according to $R(t^*)$ do have a satisfactory aggregated reliability, making this set to be the top 15%.

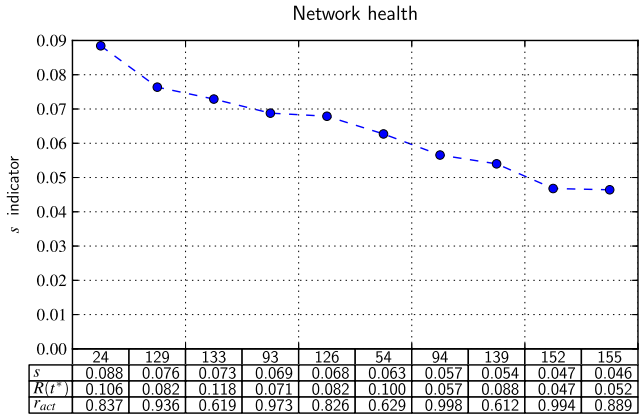

	24	129	133	93	126	54	94	139	152	155
s	0.088	0.076	0.073	0.069	0.068	0.063	0.057	0.054	0.047	0.046
$R(t^*)$	0.106	0.082	0.118	0.071	0.082	0.100	0.057	0.088	0.047	0.052
r_{act}	0.837	0.936	0.619	0.973	0.826	0.629	0.998	0.612	0.994	0.889

FIGURE 11 The 10 sensors with higher s values (from a total of 33 with enough data to estimate the indicator). The numbers just below the plot are the site IDs [Colour figure can be viewed at wileyonlinelibrary.com]

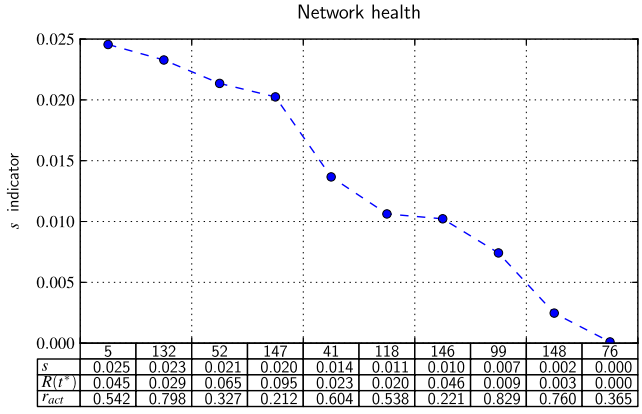

	5	132	52	147	41	118	146	99	148	76
s	0.025	0.023	0.021	0.020	0.014	0.011	0.010	0.007	0.002	0.000
$R(t^*)$	0.045	0.029	0.065	0.095	0.023	0.020	0.046	0.009	0.003	0.000
r_{act}	0.542	0.798	0.327	0.212	0.604	0.538	0.221	0.829	0.760	0.365

FIGURE 12 The 10 poorest performing sensors in terms of s. Notice the difference between this scale and the one in Figure 11 [Colour figure can be viewed at wileyonlinelibrary.com]

Then, in this case, for this data, indicator, noise threshold, and according to our criteria of the top 15% of sensors, we can say that the sensors with an aggregated reliability value over 0.09 are performing well.

Now, consider Figure 6: The lowest 15% sensors reveal $R(t^*) \leqslant 0.025$. Then, in this case, one could determine that sensors that have a reliability below that value should be examined.

Note that using another t^* will change the results. In particular, studying the network with $t^* < 0.5$ hours will rise the reliability value of every sensor, and possibly change the ranking.

For reference, in Figure 9, we present the aggregated reliability of every active sensor with suitable data to calculate the indicator.

7.2 | Ratio of activations: r_{act}

In this case, we have some sensors that almost reach the theoretical max $\{r_{\text{act}}\} = 1$. According to our method on this particular data, these sensors perform very well in the sense of registering the microseisms that they are supposed to record. Looking at Figure 7, the top 15% (10 sensors) have $r_{\text{act}} \geqslant 0.8$.

Depicted in Figure 8 are the lowest 15% of sensors. Compared to the best ones, they have very low values for r_{act}, revealing $r_{\text{act}} \leqslant 0.08 \ll 0.8$. In this case, these sensors rarely register a microseism when they have to, so the recommendation is that they should be examined.

For reference, in Figure 10, we present the ratio of activations of every active sensor that passes the requirements to have this indicator calculated.

7.3 | Performance: *s*

We propose the performance indicator *s* to evaluate the health of the network's sensors, which give us a quick way to get the big picture of their conditions.

For example, consider sensors 24 and 129. According to Figure 11, they are the best performing sensors overall, so we expect them to have both high reliability and ratio of activations. This can be verified in Figures 5 and 7, respectively. In both cases, they are on the top 15%: 2nd and 8th in terms of $R(t^*)$, and 9th and 6th in terms of r_{act}, respectively.

On the other hand, we have the case of poor-performing sensors. Take for example sensor 148 that, according to Figure 6, is second-to-last in terms of $R(t^*)$. However, it performs adequately in terms of r_{act}, ranking 20th out of 66 (not pictured). Nevertheless, its reliability is so poor, that it is second-to-last in terms of *s*.

Another example concerning low-*s* sensors is the case of sensor 147, which ranks 27th out of 33 in terms of performance (depicted in Figure 12). But, as the results show, this does not mean that this sensor is performing poorly in both indicators: Actually, it has a high reliability, ranking 4th on that indicator (depicted in Figure 5). Nonetheless, it performs poorly in terms of the ratio of activations, ranking 54th out of 66, low enough to be in the bottom 15% according to *s*.

The *s*-indicator gives us a quick way to explore the results. When a sensor ranks low on that indicator, it is important to explore the details behind its value—the reliability and ratio of activations—and act accordingly.

8 | FURTHER RESEARCH LINES

Given that our method is sensitive to some of the chosen parameters (eg, noise thresholds and the radius of the sphere), finding a robust way to compute them would increase its advantages.

In particular, there is room for improvement in the construction of the volume that is needed to calculate the ratio of activations. The spherical volume approach used here might not suitably take into account the physics behind the phenomenon as close as desired. Also, the estimation of r_{act} is highly dependent on the radius of this sphere, which reinforces the need for a robust methodology to compute it.

The method can also be enhanced by designing an algorithm to choose the noise threshold, in terms of the optimization of a suitable objective function.

Also, the way to compute the equivalent reliability was mainly based upon simplicity considerations, and so it could be changed for a better or more informative one if other criteria are to be taken into account.

9 | CONCLUSION

In this paper, we presented a nondisruptive method to deal with the problem of monitoring the health of a remote-sensing network. Our approach differs from the ones available in the literature and furnishes a novel formal framework, based on reliability engineering, to deal with seismic network health monitoring.

We focus on evaluating the performance of the sensors themselves, quantifying how different noise sources possibly result into false microseisms detections (which can be seen as the network making a Type I error) and pointing out what sensors are not registering the data they are supposed to record (in analogy with a Type II error). With these ideas in mind, we defined several quantitative indicators of the performance of each sensor, namely, reliability, ratio of activations and an aggregated indicator of both of them, which can then be used to compare or rank the sensors according to the chosen performance criteria.

The method we propose to evaluate the network's health uses data that are already available as part of the ongoing measurement process. Thus, the method does not interfere with it nor requires the installation of new equipment or being included explicitly in the design phase of the project. Moreover, it can be programmed to work automatically, scheduling the generation of reports which later can be evaluated by experts.

The results of our procedure must be analyzed in their context. Indeed, the values obtained for each sensor are not important on their own but should rather be compared to the values obtained by the other sensors, and taking always into account the global measuring performance of the network.

We applied our methodology to the data registered by El Teniente's seismic network on September 8, 2010. In this case, since the network is known to satisfactorily accomplish its task, we looked for the worst 15% of sensors according to the performance index *s* and recommended the examination of their corresponding values of reliability and ratio of activations.

The implementation of this method, including the thresholds that are considered as well as the interpretation of the results, should be done consciously, and always in collaboration with experts in the network operation, who should ultimately evaluate the reasons of the relative poor performance of a given sensor and then proceed accordingly to solve the problem.

ACKNOWLEDGEMENTS

This work was partially founded by Codelco Chile, División El Teniente and the Basal-Conicyt Grant "Center for Mathematical Modeling" (CMM), Universidad de Chile.

REFERENCES

1. Ge M. Efficient mine microseismic monitoring. *Int J Coal Geol*. 2005;64(1):44-56.
2. Mendecki AJ, van Aswegen G, Mountfort P. A guide to routine seismic monitoring in mines. In: *A Handbook on Rock Engineering Practice for Tabular Hard Rock Mines, chapter 9*, Jager AJ, Ryder JA eds. The Safety in Mines Research Advisory Committee: Johannesburg; 1999; 287-309.
3. Kothamasu R, Huang SH, VerDuin WH. *Handbook of Maintenance Management and Engineering*, chapter 14: System Health Monitoring and Prognostics—A Review of Current Paradigms and Practices. London, Springer: London, 2009;337-362.
4. Meng X, Nandagopal T, Li L, Lu S. Contour maps: Monitoring and diagnosis in sensor networks. *Comput Netw*. 2006;50(15):2820-2838.
5. Mengshoel OJ, Darwiche A, Uckun S. Sensor validation using Bayesian networks. In: *Proc. 9th International Symposium on Artificial Intelligence, Robotics, and Automation in Space (iSAIRAS-08)*, Los Angeles, CA, USA 2008.
6. Pearl J. *Probabilistic Reasoning in Intelligent Systems: Networks of Plausible Inference*. Morgan Kaufmann Publishers Inc.: San Francisco, CA USA, 1988.
7. Elouedi Z, Mellouli K, Smets P. Assessing sensor reliability for multisensor data fusion within the transferable belief model. *IEEE Trans Syst Man Cybern Part B Cybern*. 2004;34(1):782-787.
8. Smets P, Kennes R. The transferable belief model. *Artif Intell*. 1994;66(2):191-234.
9. Xie J, Pecht M. Applications of in-situ health monitoring and prognostic sensors. In: *9th Pan Pacific Microelectronics Symposium Exhibits & Conference*: Kahuku, Oahu, Hawaii, 2004;10-12.
10. Cannell J, Cooke DR, Walshe JL, Stein H. Geology, mineralization, alteration, and structural evolution of the El Teniente porphyry Cu-Mo deposit. *Econ Geol*. 2005;100(5):979-1003.
11. Vallejos JA, Brzovic A, Lopez C, Bouzeran L, Mas Ivars D. Application of the synthetic rock mass approach to characterize rock mass behavior at the El Teniente Mine, Chile. In: Proceedings of the 3rd International FLAC/DEM Symposium, Hangzhou, China 2013;07-02.
12. Birolini A. *Reliability Engineering, Theory and Practice*. Springer-Verlag: Berlin Heidelberg, 2014.
13. Weibull W. A statistical distribution function of wide applicability. *ASME J Appl Mech*. 1951;18:293-297.
14. Prabhakar Murthy DN, Bulmer M, Eccleston JA. Weibull model selection for reliability modelling. *Reliab Eng & Syst Saf*. 2004;86(3):257-267.
15. Shumway RH, Stoffer DS. *Time Series Analysis and Its Applications: With R Examples*. Springer: New York, 2011.
16. Nuttall AH. Some windows with very good sidelobe behavior. *IEEE Trans Acoust Speech Signal Process*. 1981;29(1):84-91.
17. Stoica P, Moses RL. *Spectral Analysis of Signals*, Pearson Prentice Hall: Upper Saddle River, NJ, 2005.
18. Oppenheim AV, Schafer RW, Buck JR. *Discrete-Time Signal Processing*. Pearson Prentice Hall: Upper Saddle River NJ, 1999.
19. Kirlin RL, Done WJ. Covariance analysis for seismic signal processing. Society of Exploration Geophysicists Tulsa, OK 1999.
20. Robert C, Casella G. *Monte Carlo Statistical Methods* 2nd ed. Springer-Verlag: New York, 2004.
21. Ata MY. A convergence criterion for the Monte Carlo estimates. *Simul Model Pract Theory*. 2007;15(3):237-246.
22. Hirose H. Bias correction for the maximum likelihood estimates in the two-parameter Weibull distribution. *IEEE Trans Dielectr Electr Insul*. 1999;6(1):66-68.
23. Hastie T, Tibshirani R, Friedman J. *The Elements of Statistical Learning: Data Mining, Inference, and Prediction* 2nd ed. Springer-Verlag: New York, 2009.
24. D'Agostino RB, Stephens MA. *Goodness-of-fit Techniques*, vol. 68. Marcel Dekker, Inc.: New York, NY, USA, 1986.
25. Newby MJ. The properties of moment estimators for the Weibull distribution based on the sample coefficient of variation. *Technometrics*. 1980;22(2):187-194.

How to cite this article: Neira D, Soto G, Fontbona J, Prado J, Gaete S. A nondisruptive reliability approach to assess the health of microseismic sensing networks. *Appl Stochastic Models Bus Ind*. 2018;34:261–277. https://doi.org/10.1002/asmb.2266